Peer-reviewed version available at Coatings 2019, 9, 803; doi:10.3390/coatings9120803

Article

Photocathodic Protection of Cobalt Doped ZnO Nanorod Arrays for 316 Stainless Steel and Q235 Carbon Steel in 3.5 wt.% NaCl Solution

Xiong Zhang [1], Guanghui Chen [2], Weihua Li [3], Dianwu Wu [1,*]

[1] School of Materials Science and Engineering, Tongji University, No. 4800 Caoan Road, 201804, Shanghai, P.R. China; e-mail: zhangxiong@tongji.edu.cn

[2] College of chemical engineering, Qingdao University of science & technology, No.53 Zhengzhou Rd, 266042, Qingdao, P. R. China; e-mail: guanghui@quest.edu.cn

[3] School of Chemical engineering and technology, Sun Yat-Sen University Zhuhai Campus, tangjiawan, 519082, Zhuhai, P.R. China; e-mail: liweihua3@mail.sysu.edu.cn

* Correspondence: School of Materials Science and Engineering, Tongji University, No. 4800 Caoan Road, 201804, Shanghai, P.R. China; e-mail: wdw110044@163.com

Abstract: In this work, cobalt doped ZnO nanorod arrays with anticorrosion function were successfully prepared on FTO substrate by a simple aqueous solution method. XRD and EDS indicate the doped Co^{2+} has successfully incorporated into the ZnO crystal lattice. Photocurrent density and open circuit potential (OCP) results indicate the photocathodic protection performance for 316 stainless steel (316 SS) and Q235 carbon steel in 3.5 wt.% NaCl solution under 300 W Xe lamp enhanced with the increase of cobalt concentration, and the photoanode with 15% Co/Zn ratio has the optimal photocathodic protection effect. The mechanism of enhancement may be result from the narrowed band gap, the lower recombination rate of photogenerated electron-holes, the intermediate impurity level and the split of the hypo-outer shell of cobalt ions.

Keywords: cobalt; ZnO; photocathodic protection; corrosion protection

1. Introduction

Metal corrosion is a spontaneous process which the gibbs free energy of the metal has been lowered and the metal return to its stable state in nature. However, corrosion caused great losses, including economic, environmental damages, life, injury and efficiency, et al. Among several corrosion control strategies, impressed current cathodic protection is not suitable for remote places, sacrificial anode protection consumes abundant of resources every year, and the coating can not tolerate few breakages which may accelerate the rate of corrosion. Therefore, it was urgently for us to find a sustainable and environmentally friendly technology for corrosion control. Photocathodic protection was studied extensively recent years, the principle is that the electrons in *n*-type semiconductors are excited by solar light with certain wavelength and transfer to the metal in a direct or indirect manner, which was equivalent to the impressed current cathodic protection, and result in the cathadically polarization of the metal. Photocathodic protection was originally found from the emergence of electron-hole pairs in TiO_2 film when irradiated by ultraviolet light [1], and the OCP of the coupled metal shifted to the negative potential, which lowered and even stop the corrosion of the coupled metal. The biggest advantage of photocathodic protection is that photocathodic protection is a green, sustainable and one of the most promising anticorrosion

methods, which originate from the use of clean and inexhaustible solar energy for the corrosion protection.

Up to now, most studies with regards to photocathodic protection system focus on anodic oxidation prepared TiO_2 and its composites with other semiconductors for the anticorrosion of stainless steel [2-5]. Due to the low electron mobility, the photocurrent density of pure TiO_2 coupled with 304 SS was smaller than 50 μA/cm², and the polarized OCP was ~ -450 mV. Through modified with other semiconductors, the photocathodic protection properties have greatly improved. The 3D $ZnIn_2S_4/TiO_2$ composite has increased the photocurrent density of the coupled 304 SS greater than 2.0 mA/cm², and the polarized OCP was negative shifted to about -1.17 V. The photocurrent density of $ZnS\text{-}Bi_2S_3/TiO_2/WO_3$ film coupled 403 SS was about greater than 110 μA/cm², and the OCP was to about -520 mV. The study of $ZnIn_2S_4$/RGO/TiO_2 composites for the photocathodic protection of Q235 (the rarely reported photocathodic protection for carbon steel) possessed the photocurrent density of 5.6 mA/cm² and OCP of -1.1 V, which can provide adequate protection for Q235. However, most of the modified semiconductors were sulphides which often suffer from the photocorrosion due to the instability of S^{2-}.

Zinc oxide (ZnO) is a semiconductor material with wide band gap of about 3.2 eV, which was widespread used in photocatalysis [6], dye-sensitized solar cell [7], photoluminescence [8] and electronic device [9], due to its abound in natural resources, low price and environmental friendly [10-11]. Besides, ZnO has high electron mobility which was two orders of magnitude higher than TiO_2 [12], ZnO might be an appropriate photoanode in photocathodic protection system. It is well known that doping a selective element into ZnO is an effective route to improve the optical and electrical properties, and to increase the carrier concentration, because a higher carrier concentration is required. Transition metal (TM) such as Co, Fe, Ni, and Mn doping into ZnO may increase the carrier concentration due to the impurity energy level or another introduced intermediate level [13] which may lower the requirement for the wavelength of the light and promote the efficiency of the photocathodic protection for the metals.

In this article, we successfully prepared ZnO nanorod arrays on FTO substrate with different cobalt doping concentrations by a simple aqueous solution method. The morphology, optical, and photocathodic protection properties of as-prepared ZnO nanorod arrays were all changed with the change of cobalt concentrations.

2. Experimental

All of the chemical reagents used in this study were analytical reagents and without further purification. All of the aqueous solutions were prepared using double distilled water.

2.1. Preparation of ZnO nanorod arrays

ZnO nanorod arrays were prepared by aqueous solution method. Firstly, clean the substrate. FTO (≤10 Ω/sq, 10 mm × 13 mm) substrates were ultrasonic cleaned with deionized water (DI water) acetone, ethanol, and DI water for 30 min, respectively. Then dried in the vacuum drying oven at 80°C for 30min. Secondly, in order to the benefit of the uniform growth of ZnO nanorod arrays, ZnO nanoparticles were coated on the FTO substrate. The well cleaned FTO substrates were spin coated by a spin coater, the zinc nitrate hexahydrate ($Zn(NO_3)_2{\cdot}6H_2O$) and hexamethylenetetramine ($C_6H_{12}N_4$, HMT) aqueous solution were used as the precursor, the spin parameter was set to third

gears. The velocities were 500 r/min, 2000 r/min, and 5000 r/min respectively, and the rotation time of each gear were all 10 s. After that, the substrate was sintered in a muffle furnace at 450°C for 10 min. This porcess was repeated for three times in order to form the uniform ZnO seed film on the substrate. Thirdly, ZnO nanorod arrays were grown vertically by immersing the cleaned FTO substrate in the aqueous solution of $Zn(NO_3)_2{\cdot}6H_2O$ (0.025M), HMT (0.025M) and different concentrations of cobaltous acetate tetrahydrate ($Co(CH_3COO)_2{\cdot}4H_2O$). The reaction temperature and time were set at 80°C and 12 h in the water bath, then rinsed thoroughly with DI water for several times to eliminate residual salts, and dried for 1.0 h at 80°C. On the basis of the different concentrations of $Co(CH_3COO)_2{\cdot}4H_2O$, the dopant concentrations of cobalt in the reactive solution were 0, 1.25, 2.50, 3.75, 5.00 mM, respectively, corresponding to the Co/Zn ratio of 0%, 5%, 10%, 15%, 20%, respectively. The as-prepared ZnO samples are labeled as C0, C1, C2, C3 and C4 in the subsequent discussion in this paper, respectively.

2.2. Characterization

Morphological characterization was performed on a scanning electron microscopy (SEM, ZEISS EV018). The composition was determined by an Energy Dispersive Spectrometer (EDS, Bruker XFlash 6130). The crystalline structures of the samples were recorded by X-ray diffraction (XRD, Bruker AXS D8 ADVANCE) with a copper X-ray source (Cu–Kα, 50 kV, 250 mA). The reflectance spectra were performed with an Agilent Cary 5000 UV-Vis-NIR spectrophotometer, and MgO powder was served as the reference material. The photoluminescence (PL) spectra were performed with a fluorospectrophotometer (Hitachi F-4600). The OCP and photocurrent density of the photoanodes were performed on an electrochemical workstation (Gamry Reference 3000).

2.3. Electrode fabrication and photoelectrochemical measurements

Metal electrode: Here, we chose the wildly used steel (316 SS and Q235) to be the object of our research. First, the cube metals (10 mm × 10 mm × 10 mm, the element content were shown in **Table 1**) were polished with sand paper of 600, 1200 and 2000 mesh in sequence on a metallographic polishing machine. Second, to ensure good contact, the cube iron was connected with copper wire by tin welding. Third, keep one side of the cube iron (to be studied) exposed, encapsulate the other sides and the welded joint with ethoxyline resin in case of corrosion. Before examination, polish the exposed side of cube iron every time to ensure the consistency and veracity of the results.

Table 1. The element content of 316 SS and Q235

Type	C	Mn	Si	S	P	Ni	Cr	Mo
316 SS	0.08	1.80	0.90	0.029	0.045	14.00	17.00	2.00
Q235	0.19	0.59	0.30	0.05	0.44	-	-	-

Photoanode: First, cut out ZnO/FTO substrate with a certain size (10 mm × 13 mm, including 10mm × 3 mm blank FTO with no ZnO film). Second, connect the conductive side of FTO with the copper wire by silver conductive adhesive. Third, encapsulate the blank FTO and the connected joint with ethoxyline resin.

Photoelectrochemical measurements: The diagrammatic sketch of the experiment setup is shown in Figure 1. The experiment setup is a double electrolytic cell system which is composed of a photoelectric cell and a corrosion cell. The photoelectrodes and metal electrodes (316SS and Q235) were put into the photoelectric cell and corrosion cell, respectively. The electrolyte in the

photoelectric cell is Na_2S (0.1 M) and Na_2SO_3 (0.1 M). The electrolyte in the corrosion cell is simulated seawater solution (3.5 wt.% NaCl). The measurements of OCP and photocurrent density were conducted by Zero Resistance Ammeter (ZRA mode) on Gamry Reference 3000. The photoelectrode was connected with the work electrode (WE) and working sense electrode (WSE), the metal electrode was connected with the current electrode (CE) and current sense electrode (CSE), and the saturated calomel electrode (SCE) served as the reference electrode (RE). The measurements were carried out under simulated solar light source with a 300 W Xenon lamp (Microsolar 300, Beijing Bofeilai Co.). All electrochemical measurements were performed at ambient temperature.

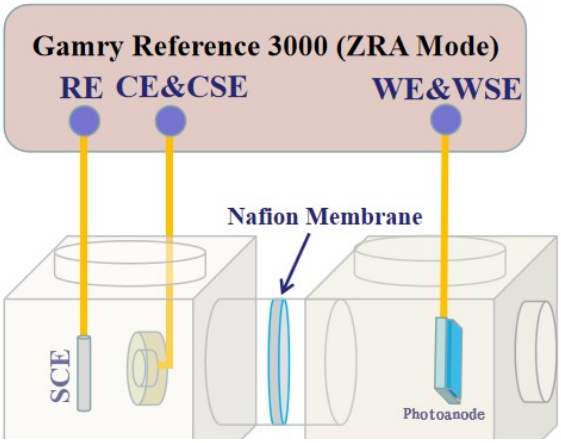

Figure 1. Schematic diagram of the double electrolytic cell setup for the measurement of OCP and photocurrent density.

3. Results and Discussion

3.1. Morphology and crystal structure analysis

Figure 2 shows SEM images of the pure and cobalt doped ZnO nanorod arrays grown on FTO substrate. All ZnO samples are regular nanorod shaped from the appearance, and the nanorods are all hexagonal prisms. From the sectional view images of C0 in Figure 2 (a), the one-dimensional ZnO nanorods have vertically grown on the FTO substrate with ZnO seed layer, the length of pure ZnO nanorod is about 1.5 μm, and the thickness of ZnO seed layer is about 200 nm. From Figure 2 (b-f), the nanorod diameter of each sample is not uniform, and the average diameter of ZnO nanorods are about 80 nm, 80 nm, 80 nm, 95 nm, and 120 nm for C0, C1, C2, C3, and C4, respectively, which indicate the diameter of ZnO nanorod is get larger with the increase of cobalt in precursor.

The composition of ZnO samples are determined by EDS in Figure 3 (a), and the result shows the existence of Zn, O, Sn, Si, Co, and C in the spectrum. The elements of Sn, Si, and C are ascribed to the FTO substrate that ZnO nanorod arrays grown on, and the element Zn and O formed ZnO. The existence of cobalt suggests that cobalt has entered into the ZnO nanorod arrays. Table 2 shows the

Table 2. Cobalt concentration in ZnO nanorod arrays determined by EDS analysis

Sample	C1	C2	C3	C4
Co%	<1	2	6	4.5

cobalt concentration in doped ZnO nanorod arrays determined by EDS, there are 2%, 6%, and 4.5% cobalt ions doped into ZnO in C2, C3, and C4 samples, respectively, which implies the actual

quantities of cobalt in ZnO is far less than the quantities of cobalt precursor, and C3 has the maximum cobalt doping concentrations.

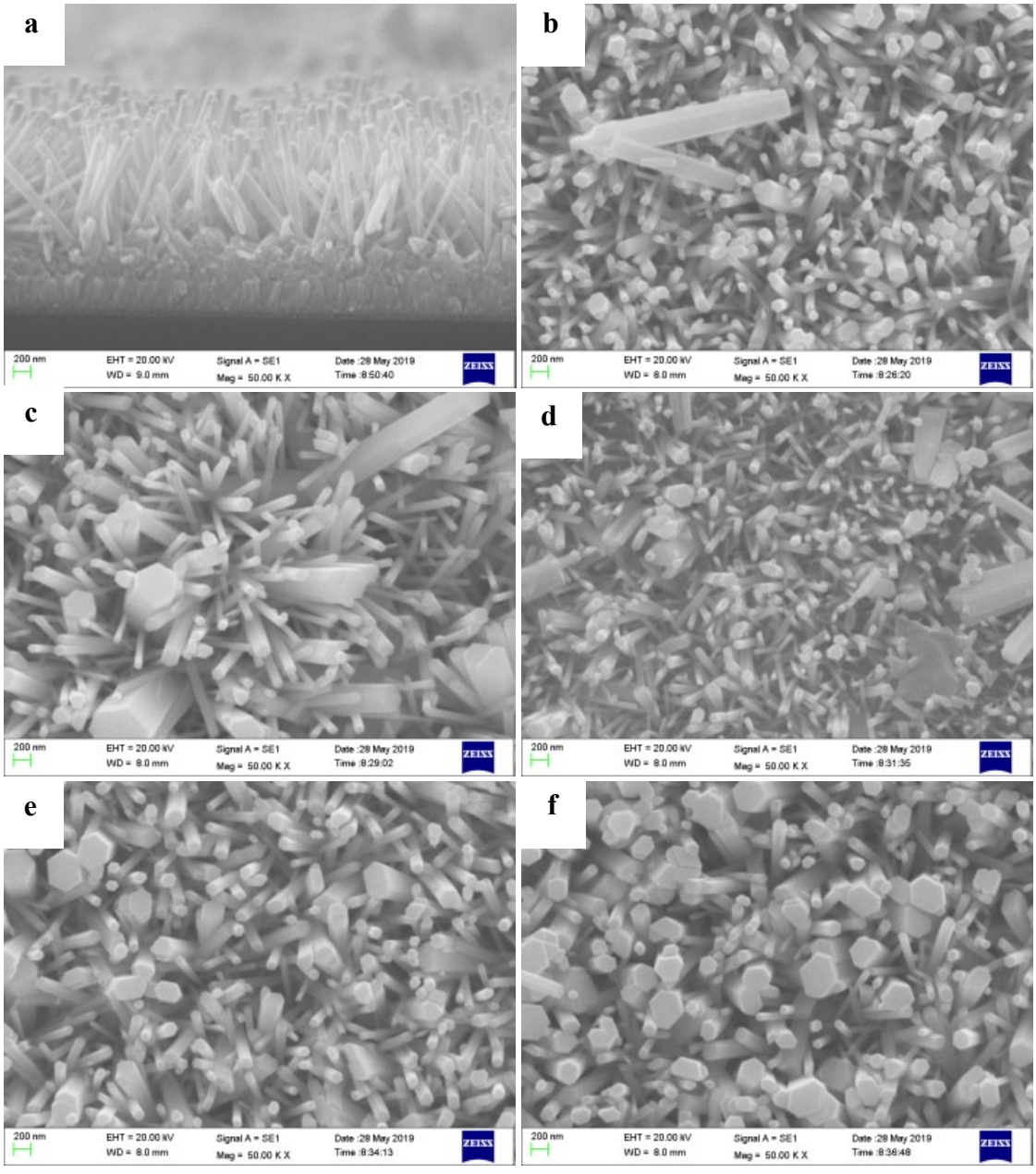

Figure 2. SEM images of ZnO nanrod arrays grown on FTO substrate with different cobalt doping concentrations. (a) sectional view of C0. (b) C0. (c) C1. (d) C2. (e) C3. (f) C4.

In order to confirm that the dopants were doped into the crystal lattice of ZnO rather than formed the oxide of the dopant, XRD was performed. Figure 3 (b) displays the XRD patterns of the as-prepared pure and doped ZnO films. All ZnO diffraction peaks are in good agreement with the JCPDS card (No. 36-1451) for a typical wurtzite-type ZnO crystal (hexagonal). These peaks at scattering angles (2θ) of 32.06°, 34.76°, 36.56° and 47.84°, correspond to the diffractions from the (100), (002), (101), and (102) of the ZnO hexagonal phase, respectively. The (002) diffraction peaks of cobalt doped ZnO nanorod array, compared to pure ZnO nanorod arrays, a slightly left-shifted by about 0°, 0.2°, 0.2° and 0.3° for C1, C2, C3, and C4 samples, respectively. The c-axis lattice parameter

decreased with the dopant incorporated into the crystal lattice. No other diffraction peaks were detected, implying that there were no CoO, Co_2O_3 or Co_3O_4 crystal structures in the doped samples.

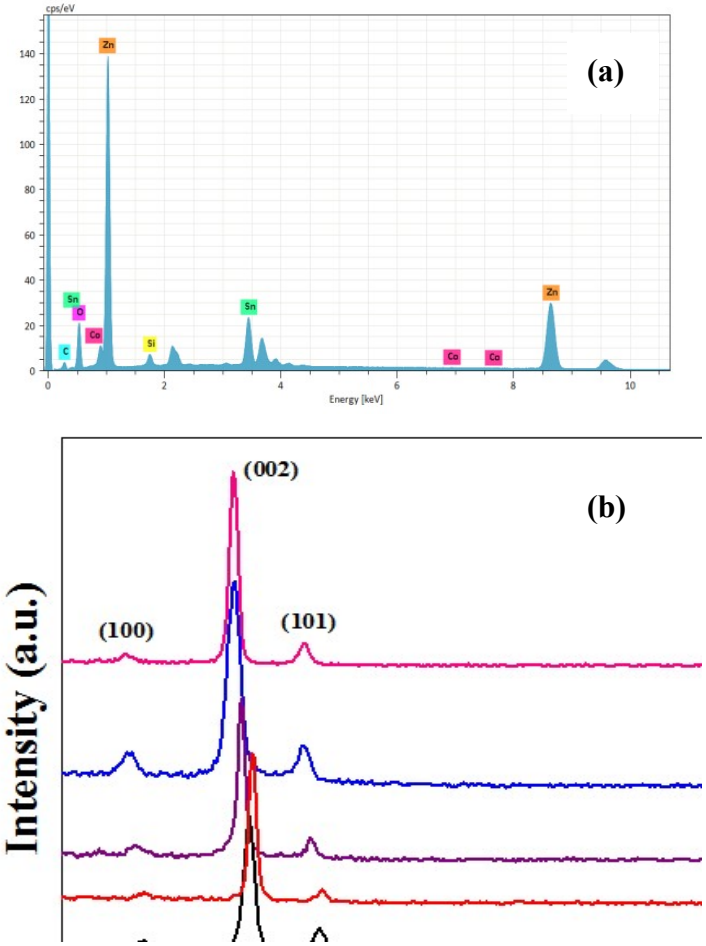

Figure 3. (a) EDS and (b) XRD patterns of cobalt doped ZnO nanorod arrays.

3.2. Optical properties analysis

Figure 4 (a) shows the UV-Vis diffuse reflectance spectra of different cobalt doped ZnO nanorod arrays. The absorption band-edge of pure ZnO is at approximately 390nm, and with the increase of cobalt concentration, the absorption band-edges are slightly red-shifted. C3 has the largest red-shifted range. Compared to the relative lower absorption intensities in ultraviolet range, the cobalt doped ZnO nanorod arrays had higher light absorption intensities in visible light range (more than 400 nm), which means the ability of utilizing visible light has promoted.

The band gap of the photoanode could be roughly estimated by the following equation for a semiconductor [14]: $\alpha h\nu = A(h\nu - E_g)^{\eta}$, where α, h, ν, A , E_g and η represent the optical adsorption coefficient, the Planck constant, the frequency of light, a constant, the band gap of semiconductor and a characteristic of the type of electrons transition process ($\eta = 1/2$ for a direct semiconductor, $\eta = 2$ for an indirect semiconductor). From Figure 4 (b), the estimated band gap values of C0, C1, C2, C3 and C4 films were approximately 3.23 eV, 3.20 eV, 3.19 eV, 3.17eV and 3.18 eV, respectively. The band gap became slightly narrowed when the cobalt doping in ZnO.

Figure 5 displays the typical PL spectra of different dopant concentration of ZnO nanorod arrays. The PL spectra includes three peaks: an UV emission peak which is located at 390 ~ 400 nm,

Preprints (www.preprints.org) | NOT PEER-REVIEWED | Posted: 29 October 2019 doi:10.20944/preprints201910.0332.v1

Peer-reviewed version available at Coatings 2019, 9, 803; doi:10.3390/coatings9120803

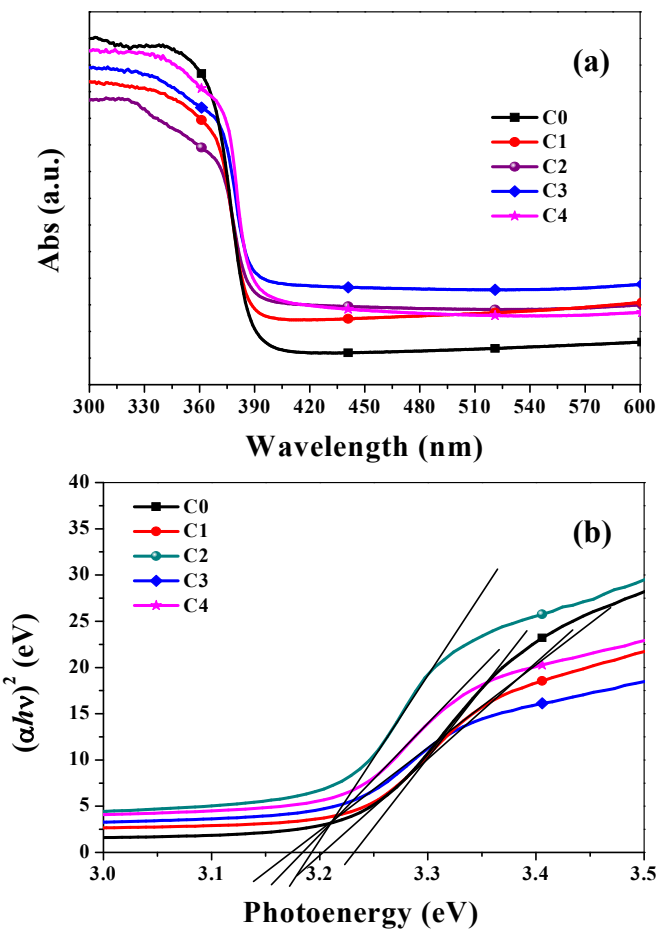

Figure 4. (a) UV-Vis absorption spectra of pure and cobalt doped ZnO nanorod arrays measured at room temperature. (b) Plots of (αhν)1/2 vs. photoenergy for the pure and cobalt doped ZnO nanorod arrays.

a distinct shoulder peak located at ~ 460 nm, and an unobvious weak green emission band located at ~ 530 nm, respectively. The peak in UV range belongs to the excitons recombination corresponding to near-band-edge emission of the ZnO [15]. The point of each photoanode's UV-emission peak was signed in the spectra with arrows, and it can be clearly observed that the UV-emission peaks were red-shifted by 2.0, 8.0, 10.0, and 2.0 nm for C1, C2, C3, and C4 compared to the pure ZnO, respectively. This indicates that the band gap became a bit narrow with the increase of the doping Co concentrations till Co/Zn ratio of 15%, and the band gap turned larger when Co/Zn ratio is 20%. With the increase of Co concentration (Co/Zn ratio from 0 to 15%) in ZnO, the UV-emission peaks are obviously getting weaker, it illustrates the near band edge emission which caused by the recombination of photogenerated electron-hole pairs was weaker, and the recombination of charge carrier has been depressed. The green emission peaks located at 530 nm have been reported to be ascribed to the internal defect in crystals (oxygen vacancies) and the transition of a photogenerated electron from a dark level below the conduction band to a deeply trapped hole [16]. We know that that some dopants or defects in semiconductors tend to generate one or more deep energy level, which can not only capture electrons, but also capture holes, and these defects might be the recombination center in semiconductors. The recombination center can promote the recombination of the photogenerated electron-holes, and will release energy in the form

of fluorescence. As shown in Figure 5, with the increase of the doping Co concentrations, the defects in the photoanodes increased, and the corresponding intensities of the green emission peaks located at 530 nm enhanced. It is not good for the utilization of the generatated electrons. On the other hand, the recombination center between the valence band and the conduction band turns to be an intermediate energy level. The electrons on the valance band could be excited to the intermediate energy level first, and then excited to the conduction band, leaving holes in the valence band meanwhile. No matter the energy between the valence band and the intermediate energy level or the energy between the intermediate energy level and the conduction band is much less than the E_g of ZnO. The recombination center plays a role of a "step", and the electrons can be excited by a relative small energy through this "step". In other words, the electrons can be excited by the light of shorter wavelength, and it can be verified by UV-Vis Abs spectra (Figure 4) that the absorption intensity of cobalt doped ZnO nanorod arrays becomes stronger when the wavelength exceed 400 nm.

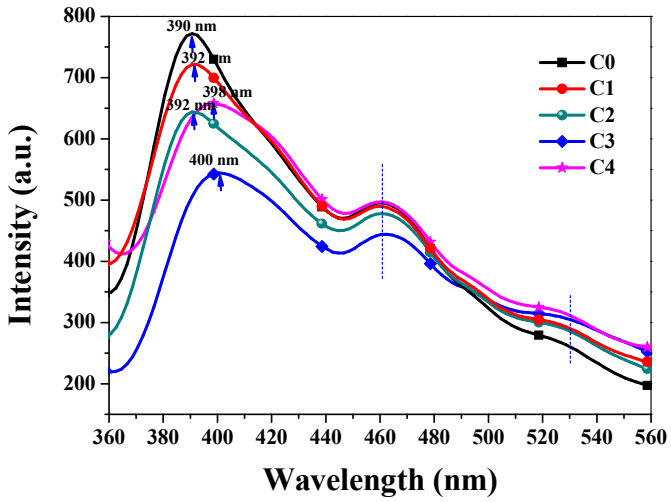

Figure 5. PL spectra of pure and cobalt doped ZnO nanorod arrays.

3.3. Photocathodic protection properties

In order to validate the photocathodic protection properties of the doped ZnO samples, the OCPs and photocurrent densities of the galvanic couple between 316 SS electrode and different photoanodes under intermittent simulated sunlight in 3.5% NaCl solution were measured. In the light of the principle of the cathodic protection for metal protection, the potential of the coupled metal will quickly polarize when impressed galvanic current, and the metal corrosion potential will lower to the protective potential. As shown in Figure 6 (a), all samples have a relatively small photocurrent densities (lower than 10 μA/cm²) under dark condition, and the photocurrent densities were all rapidly increased owing to the photoelectric effect once the light switched on, which indicates that the photogenerated electrons originate from the photoanode flow to the metal electrode. After switching off the light, the photocurrent all return to the initial position (dark condition), and once the light switched on again, the photocurrent were all rapidly increased again. After four times circulation, the value of the photocurrent densities is as follows: C3 (136.27μA/cm²) > C4 (110.41 μA/cm²) > C2 (97.88 μA/cm²) > C1 (68.23 μA/cm²) > C0 (42.69 μA/cm²). Compared with pure ZnO, the photocurrent of the cobalt doped ZnO all increased, and the photocurrent densities get larger with the increase of actual cobalt doping concentration. The value of OCP represents the

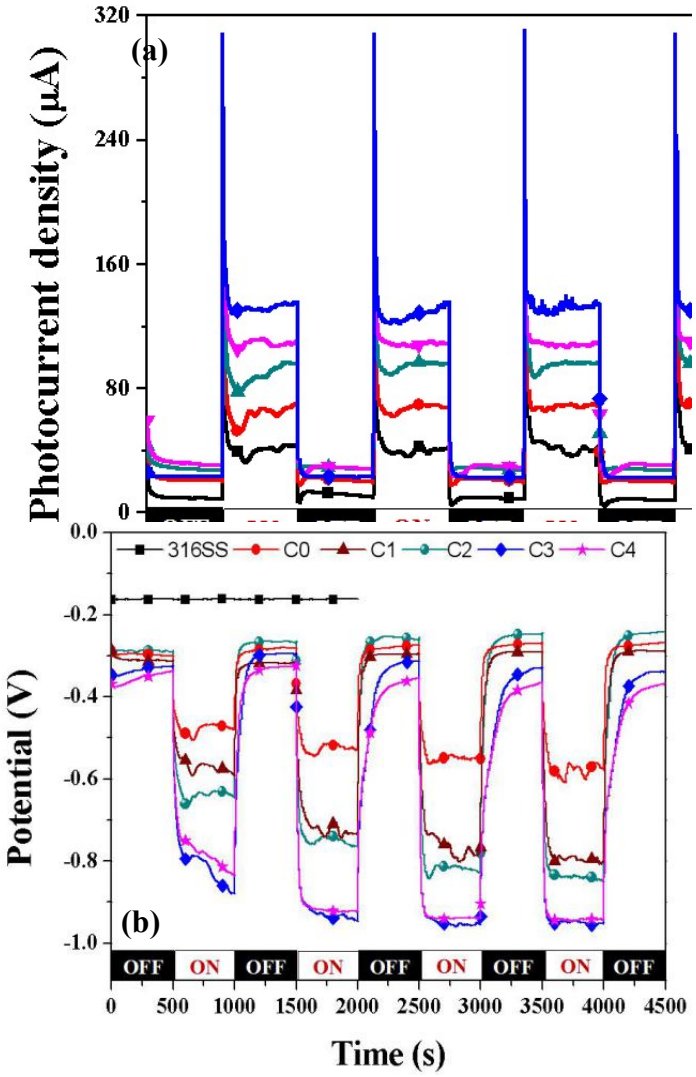

Figure 6. Photocurrent densities (a) and open circuit potential (b) of the galvanic couple of 316 SS electrode with ZnO of different cobalt doping concentration under simulated solar light switched on and off intermittently in 3.5 wt.% NaCl solution.

thermodynamics trend of metal corrosion, the more negative potential the metal has, the small probability the metal will suffer from corrosion. From Figure 6 (b), the corrosion potential (E_{corr}) of 316 SS in 3.5 wt.% NaCl solution is approximately -164 mV, and all OCPs become significantly decrease when coupling with the pure and doped ZnO photoanode films. The OCPs sharply shifted to the negative potential immediately once the light switched on, which was originated from the polarization the 316 SS caused by the impressed current (photocurrent). The OCPs were unstable at first, after manifold cycles the light switched on and off, the OCP values become relatively stable, which may be attributed to the balance between the generation and recombination of the photogenerated electron-holes [17]. According to the theory of metal polarization, the larger the impressed current is, the stronger cathodic polarization will have, and the more negative potential the metal has. As a result of the values in Figure 6 (a), C3 should have the most negative potential. From Figure 6 (b), the order of the relative equilibrium potentials of the photoandes is: C3 (-955 mV vs SCE) < C4 (-942 mV vs SCE) < C2 (-848 mV vs SCE) < C1 (-803 mV vs SCE) < C0 (-579 mV vs SCE). The OCP shifted to the original position when the light switched off, but still negative than E_{corr} of

Preprints (www.preprints.org) | NOT PEER-REVIEWED | Posted: 29 October 2019 doi:10.20944/preprints201910.0332.v1

Peer-reviewed version available at Coatings 2019, 9, 803; doi:10.3390/coatings9120803

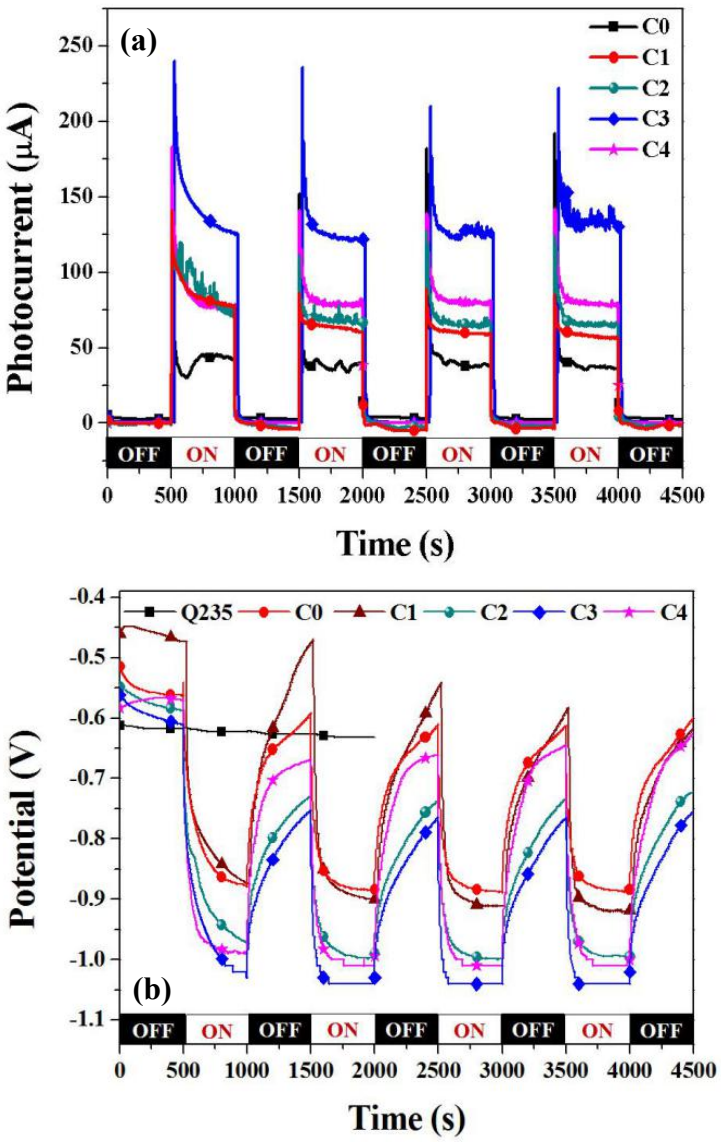

Figure 7. Photocurrent densities (a) and open circuit potential (b) of the galvanic couple of Q235 electrode with ZnO of different cobalt doping concentration under simulated solar light switched on and off intermittently in 3.5% NaCl solution.

316 SS (lower than -240 mV vs SCE). We can judge that all the pure and doped ZnO photoanodes can provide effectively protection for 316 SS, and C3 film is the best scheme.

We also tested the photocathodic protection properties of Q235 by different ZnO photoanodes. The E_{corr} of Q235 in 3.5 wt.% NaCl solution (approximately -630 mV vs SCE from Figure 7 (b)) is more negative than 316 SS, so the corrosion protection for Q235 is more difficult, and greater demands were being placed on the photoanode. Figure 7 (a) shows the photocurrent density and OCP curves of the galvanic couple between Q235 electrode with different films under intermittent simulated sunlight in 3.5 wt.% NaCl solution. Similar to 316 SS, the photocurrent density of the coupled photoanodes quickly get larger once the light switched on, and the order of the photogenerated current density of the coupled photoanodes is: C3 (133.02 μA/cm²) > C4 (78.95 μA/cm²) > C2 (65.84 μA/cm²) > C1 (56.82 μA/cm²) > C0 (36.48 μA/cm²). When coupling with different photoanodes, the OCPs of all ZnO photoanodes were higher than E_{corr} of Q235, which indicates that all ZnO photoanodes can not provide sufficient cathodic protection for Q235 under dark. When the

light switched on, the OCP sharply shifted to the negative positions which is all lower than E_{corr} of Q235, and the photogenerated current successfully gave rise to the polarize of Q235. From Figure7 (b), the order of the OCPs of the photoandes is: C3 (-1040 mV vs SCE) < C3 (-1011 mV vs SCE) < C2 (-994 mV vs SCE) < C1 (-919 mV vs SCE) < C0 (-888 mV vs SCE). We can judge that all the pure and doped ZnO photoanodes can provide effectively protection for Q235 under irradiation.

Through the test of the photocathodic protection properties of photoandes, the pure and doped ZnO have the ability of providing effective protection for 316SS and Q235. By comparison with the pure TiO_2, the polarized OCPs of stainless steel and carbon steel coupled with ZnO have the more negative potentials, and these might lead to the better protection effect upon metals. Addition with the advantage of low price and plentiful, the modified ZnO with better performance might be the appropriate photoandes for the photocathodic protection.

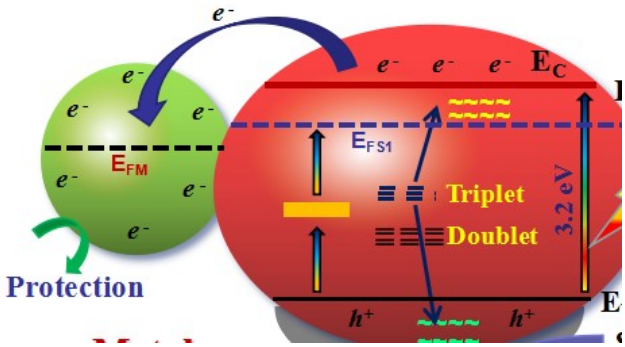

Figure 8. Schematic diagram of anticorrosion process and the photogenerated charge-transfer process in the doped ZnO coupled with metal.

3.4. Possible photocathodic protection mechanism

In order to better understand the protection mechanism of cobalt doped ZnO nanorod arrays for 316 SS and Q235, we try to analyze the reason in Figure 8 why the photocathodic protection efficiency enhanced with the increase of cobalt concentration. Normally, electrons in valence band are excited by the light, and then transfer to the conduction band, leaving holes in valence band. Some of the electrons will instantaneously neutralize with the photogenerated holes, and release energy by ways of luminescence or heat. The other electrons will migrate to the coupled metal, result in the polarization of the metal, and finally realize the protection of the metal. The holes in valence band will be consumed with the sacrificial agent (Na_2S + Na_2SO_3) in the photoelectric cell.

When cobalt doping into ZnO, firstly, the band gap of ZnO becomes slightly narrowed, and electrons can be excited by the light with shorter wavelength which may increase the number of electrons that excited from valence band to the conduction band. Secondly, the doped cobalt in ZnO can form an impurity energy level between conduction band and valence band, and the electrons can indirectly be excited to conduction via this intermediate level, which greatly lower the requirement for the energy of light. Thirdly, the hypo-outer shell of the transition metal in semiconductors is extremely prone to split. In our experiment, the introduction of Co ions in ZnO crystal lattice where Zn^{2+} locates at the center of the tetrahedron built by four oxygen atoms. The hypo-outer shell of Co (*d* state) may be confined by the tetrahedral crystal field of ZnO, and split into a higher energy triplet state and a lower energy doublet state. The triplet state hybridizes with the *p* orbital of the valence band soon afterwards and will split into two states: bonding state in the

valence band and antiboding state close to the conduction band. The bonding states will be localized and form Co-O band, and the antibonding states which possess higher energy level and some itinerant electrons have higher probability of jumping to the conduction band. Based on the explanations above, with the increase of Co concentration, the recombination probability of photogenerated electron-holes has reduced, and more electrons are possible to migrate to the conduction band to become free electrons, resulting in the increase of photocathodic protection efficiency.

4. Conclusions

Cobalt doped ZnO nanorod arrays which have good protection effect for metal have been successfully prepared by a simple aqueous solution method. The characterization results represent Co^{2+} has been successfully incorporated into the ZnO crystal lattice. The optical and photocathodic protection properties of cobalt doped ZnO nanorod arrays have been discussed, and particularly important features are as follows: UV-Vis absorption and PL spectra illustrate that the band gap and the the seperation rate of photogenerated electron-hole pairs of ZnO nanorod arrays have changed with increasing the cobalt concentrations in ZnO nanorods. OCP and Photocurrent density curves suggest that the photocathodic protection performance for 316 SS and Q235 in 3.5 wt.% NaCl solution enhanced with the increase of cobalt concentration, and the sample with 15% Co/Zn doing ratio has the optimal photocathodic protection effect. These ZnO nanorod arrays have great prospect in metal corrosion protection.

Funding: This work was financially supported by National Key R&D Program of China (2016YFC0700800).

Conflicts of Interest: The authors declare no conflict of interest.

References

1. Imokawa, T.; Fujisawa, R.; Suda, A., Tsujikawa,S. Protection of 304 Stainless steel with TiO_2 coating. *Corrosion Enigneering* **1994**, 43, 482–486.
2. Hu, J.; Guan, Z.C.; Liang, Y.; Zhou, J.Z.; Liu, Q.; Wang, H.P.; Zhang, H.; Du, R.G. Bi_2S_3 modified single crystalline rutile TiO_2 nanorod array films for photoelectrochemical cathodic protection. *Corros. Sci.* **2017**, 125, 59 – 67.
3. Guan, Z.C.; Wang, X.; Jin, P.; Tang, Y.Y.; Wang, H.P.; Song, G.L.; Du, R.G. Enhanced photoelectrochemical performances of ZnS-Bi_2S_3/TiO_2/WO_3 composite film for photocathodic protection. *Corros. Sci.* **2018**, 143, 31 – 38.
4. Sun, W.X.; Cui, S.W.; Wei, N.; Chen, S.G.; Liu, Y.P.; Wang, D.A. Hierarchical WO_3/TiO_2 nanotube nanocomposites for efficientphotocathodic protection of 304 stainless steel under visible light. *J. Alloys Comp.* **2018**, 749, 741 – 749.
5. Li, H.; Wang, X.T.; Zhang, L.; Hou, B.R. Preparation and photocathodic protection performance of CdSe/reduced graphene oxide/TiO_2 composite. *Corros. Sci.* **2015**, 94, 342 – 349.
6. Dash, P.; Manna, A.; Mishra, N.C.; Varma, S.; Synthesis and characterization of aligned ZnO nanorods for visible light photocatalysis. *Physica E* **2019**, 107, 38-46.
7. Chen, Y.C.; Li, Y.J.; Hsu, Y.K. Enhanced performance of ZnO-based dye-sensitized solar cells by glucose treatment. *J. Alloys Comp.* **2018**, 748, 382-389.
8. Borysiewicz, M.A.; Wzorek, M.; Wojciechowski, T.; Wojtowicz, T.; Kamińska, E.; Piotrowska, A. Photoluminescence of nanocoral ZnO films. *J. Lumin.* **2014**, 147, 367-371.
9. Boumezoued, A.; Guergouri, K.; Barille, R.; Rechem, D.; Zaabat, M.; Rasheed, M. ZnO nanopowders doped with bismuth oxide, from synthesis to electrical application. *J. Alloys Comp.* **2019**, 791, 550-558.

10. Huang, J.; Yin, Z.G.; Zheng, Q.D. Applications of ZnO in organic and hybrid solar cells. *Energy Environ. Sci.* **2011**, 4, 3861-3877.
11. Weintraub, B.; Zhou, Z.Z.; Li, Y.H.; Deng, Y.L. Solution synthesis of one-dimensional ZnO nanomaterials and their applications. *Nanoscale* **2010**, 2, 1573-1587.
12. Dhamodharan, P.; Manoharan, C.; Bououdina, M.; Venkadachalapathy, R.; Ramalingam, S. Al-doped ZnO thin films grown onto ITO substrates as photoanode in dye sensitized solar cell. *Solar Energ* **2017**, 141, 127-144.
13. Wu, D.W.; Huang,Z.B.; Yin, G.F.; Yao, Y.D. ; Liao, X.M.; Han, D.; Huang, X.; Gu, J.W. Preparation, structure and properties of Mn-doped ZnO rod arrays. *CrystEngComm.* **2010**, 12, 192-198.
14. Pandiyan, R.; Micheli, V.; Ristic, D.; Bartali, R.; Pepponi, G.; Barozzi, M.; Gottardi, G.; Ferrari, M.; Laidani, N. Structural and near-infra red luminescence properties of Nd-doped TiO_2 films deposited by RF sputtering. *J. Mater. Chem*. **2012**, 22, 22424-22432.
15. Wu, J. J.; Liu, S.C. Low-temperature Growth of Well - Aligned ZnO Nanorods by Chemical Vapor Deposition. *Adv. Mater.* **2002**, 14, 215-218.
16. Kim, C. G.; Sung, K.; Chung, T. M.; Jung D.Y.; Kim, Y. Monodispersed ZnO nanoparticles from a single molecular precursor. *Chem. Commun*. **2003**, 16, 2068-2069.
17. Zhou, M.J.; Zeng, Z.O.; Zhong, L. Photogenerated cathode protection properties of nano-sized TiO_2/WO_3 coating. *Corros. Sci.* **2009**, 51, 1386 – 1391.